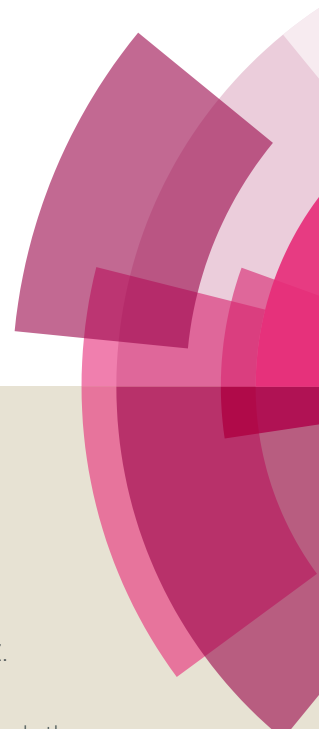


# NJC

Accepted Manuscript



This article can be cited before page numbers have been issued, to do this please use: M. Pudukudy, Z. Yaakob, Q. Jia and M. Sobri Takriff, *New J. Chem.*, 2018, DOI: 10.1039/C8NJ02842G.



This is an Accepted Manuscript, which has been through the Royal Society of Chemistry peer review process and has been accepted for publication.

Accepted Manuscripts are published online shortly after acceptance, before technical editing, formatting and proof reading. Using this free service, authors can make their results available to the community, in citable form, before we publish the edited article. We will replace this Accepted Manuscript with the edited and formatted Advance Article as soon as it is available.

You can find more information about Accepted Manuscripts in the [author guidelines](#).

Please note that technical editing may introduce minor changes to the text and/or graphics, which may alter content. The journal's standard [Terms & Conditions](#) and the ethical guidelines, outlined in our [author and reviewer resource centre](#), still apply. In no event shall the Royal Society of Chemistry be held responsible for any errors or omissions in this Accepted Manuscript or any consequences arising from the use of any information it contains.



## ARTICLE

## Catalytic decomposition of undiluted methane into hydrogen and carbon nanofilaments over Pt promoted Ni/CeO<sub>2</sub> catalysts

Manoj Pudukudy<sup>a,\*</sup> Zahira Yaakob<sup>a</sup>, Qingming Jia<sup>b</sup>, Mohd Sobri Takriff<sup>a</sup>

Received 00th January 20xx,  
Accepted 00th January 20xx

DOI: 10.1039/x0xx00000x

[www.rsc.org/](http://www.rsc.org/)

The catalytic decomposition of methane is a strategic process to produce CO<sub>x</sub>-free hydrogen and carbon nanomaterials. In this work, for the first time, highly porous ceria was prepared by a urea-assisted solid state combustion method and used as support for the preparation of a set of platinum-promoted nickel catalysts. The amount of Pt varied from 0.05% to 0.2% while retaining 20% nickel in the catalysts. The prepared catalysts were completely characterized for their structural, textural and redox properties, and their catalytic performance was tested for undiluted methane decomposition. A fine surface dispersion of nickel oxide over ceria was observed in the prepared catalysts. No peaks related to Pt were observed in the catalysts, indicating its good surface dispersion. An enhancement was observed in the properties of the Ni/CeO<sub>2</sub> catalyst after the addition of Pt as a promoter. The crystallinity of NiO was not altered by the addition of Pt, whereas the specific surface area of the catalysts was increased with the incremental addition of Pt. Furthermore, the reduction temperature of nickel oxide was shifted to low temperature in the Pt-promoted catalysts due to the hydrogen spillover effect. The surface composition and chemical states of the Pt-promoted Ni/CeO<sub>2</sub> catalysts were further studied using XPS. The Pt-promoted Ni/CeO<sub>2</sub> catalysts exhibited high catalytic efficiency for methane decomposition due to their improved catalytic properties. The addition of Pt increased the hydrogen yield, and a significant increase in the hydrogen yield was observed for the incremental amount of Pt in the catalysts. Moreover, by increasing the reaction temperature from 650°C to 750°C, the hydrogen yield increased significantly. A maximum hydrogen yield of 65% was observed for the 0.2%Pt@Ni/CeO<sub>2</sub> catalyst at 750°C. The enhanced activity and stability of the catalysts was attributed to the synergistic effects of Ni and Pt due to their fine surface dispersion over ceria with a proper metal-support interaction. Multiwalled carbon nanofilaments with different diameters were deposited over the catalysts. The carbon nanotubes deposited over Ni/CeO<sub>2</sub> catalyst were found to be more homogeneous than the Pt-promoted catalysts. Moreover, a wide hollow channel was observed in the carbon nanotubes deposited over the Pt-promoted catalyst.

### Introduction

Hydrogen is a promising zero emission fuel mainly used in fuel cells for the generation of power/electricity by its electrochemical redox reaction.<sup>1</sup> Therefore, in recent years, the production of hydrogen has attracted interest in energy research. It can be produced by several methods from various hydrogen containing sources.<sup>2</sup> Water, hydrocarbons, alcohols and biomass resources form the main sources of hydrogen. Water is the green source for hydrogen because the formation of carbon oxides is not possible from water.<sup>3</sup> Electrolysis of water and photocatalytic water splitting are the common

methods for producing hydrogen from water. However, the water-based hydrogen production methods are less effective from an industrial point of view. For instance, the electrolysis of water is associated with high cost constraints, and photocatalytic water splitting suffers the limitation of photo conversion efficiency.<sup>4</sup> In both of the aforesaid processes, the simultaneous production of oxygen provides a further hurdle for the process, because of the separation and purification of hydrogen from oxygen. Partial oxidation, autothermal reforming and steam reforming of hydrocarbons, especially methane, alcohols and biomass, are the other routes for hydrogen production.<sup>5</sup> Currently, the industrial production of hydrogen is based on the steam reforming of methane as it is an abundant source of hydrogen with a high hydrogen to carbon ratio. The simultaneous production of carbon oxides makes the route non-eco-friendly when considering environmental issues like global warming and acid rain.<sup>6</sup> Thus, it is very urgent to replace the conventional hydrogen production methods with a promising alternative method. Methane decomposition is the greener method for the production of hydrogen, since no formation of carbon oxides were observed in this anaerobic process.<sup>7</sup> Here, methane is

<sup>a</sup> Research Center for Sustainable Process Technology (CESPRO), Faculty of Engineering and Built Environment, Universiti Kebangsaan Malaysia, Bangi, 43600, Selangor, Malaysia.

<sup>b</sup> Faculty of Chemical Engineering, Kunming University of Science and Technology, Kunming 650600, Yunnan, People's Republic of China.

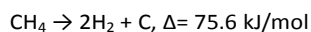
\*Email: [manojpudukudy@gmail.com](mailto:manojpudukudy@gmail.com), [manojmscp@gmail.com](mailto:manojmscp@gmail.com)

Electronic Supplementary Information (ESI) available: [details of any supplementary information available should be included here]. See DOI: 10.1039/x0xx00000x

## ARTICLE

## Journal Name

directly cracked into hydrogen and solid carbon without any other by-products. The reaction can be represented as:



The non-catalytic decomposition of methane requires high reaction temperatures of 1200°C for an efficient reaction. Also, the carbon could be deposited in the form of bulk activated carbon in its amorphous form. Because of these constraints, in the past few years, methane decomposition has been carried out in the presence of catalysts. Both metallic and carbonaceous catalysts were investigated for methane decomposition, which has a positive impact on the reaction efficiency in terms of methane conversion, product selectivity, yield and the morphology of the deposited carbon.<sup>8</sup> Moreover, the catalysts were found to enhance the reaction by reducing the reaction temperature, improving the kinetics of the process and tuning the morphology of the deposited carbon. Heterogeneous metal-based supported catalysts were highly effective for the hydrogen production and for the deposition of carbon in the form of graphene and single or multiwalled carbon nanofilaments.<sup>9</sup> These highly valuable carbon nanomaterials can be used for several applications in the field of energy, such as for hydrogen storage, electrode materials for fuel cells, supercapacitors, batteries etc.<sup>10</sup> The catalytic performance of the catalysts for methane decomposition depends on several factors. Active metals, textural promoters/supports, co-metals or promoters, synthesis methods, synthesis conditions, etc. play significant roles in determining the catalytic activity of the catalyst.<sup>11</sup> Ni, Co and Fe are the most commonly used active metals. Transition metals were used as co-metals, noble metals were used as promoters, and thermally stable metal oxides such as silica, alumina, ceria, zirconia, lanthana, magnesia, titania and their mixed compositions were used as the textural promoters.<sup>12</sup> Ceria is a rare earth metal oxide which is less studied for methane decomposition as a textural promoter.<sup>13</sup> Based on its enhanced textural and redox properties, ceria would efficiently take part in the chemical reaction by providing a surface for the dispersion of active metals and promoters. The addition of noble metals as promoters was also reported to enhance the reaction. In methane decomposition, several noble metal-promoted catalysts were reported. Many of the works focused on the type and effect of different promoters on the selectivity of the reaction and also on the carbon growth. A brief description of some of the noble metal-promoted catalysts reported in methane decomposition is discussed below.

Takenaka et al.<sup>14</sup> studied methane decomposition over Cu-, Rh-, Pd-, Ir- and Pt-promoted nickel catalysts and reported that the addition of Pd reduced the deactivation of the Ni/SiO<sub>2</sub> catalyst, whereas the addition of other promoters decreased the carbon yield. Additionally, due to the formation of Pd-Ni bimetallic alloys, an increase in the carbon yield and an improvement in the morphology of the deposited carbon nanofibers were noted. In Pd catalysts, the methane decomposition was reported to proceed through the adsorption desorption mechanism at the Pd-interacting

phases.<sup>15</sup> Ogihara et al.<sup>16</sup> studied Pd and Rh-promoted Ni, Co and Fe-loaded alumina catalysts for methane decomposition. As per their study, among the various catalysts synthesized, the Pd-Co/Al<sub>2</sub>O<sub>3</sub> catalyst showed the highest carbon yield at 740°C, and the catalyst provided a maximum hydrogen yield of 94% at a reaction temperature of 850°C. Ruthenium- and Platinum-promoted Fe/SiO<sub>2</sub> catalysts were also used for methane decomposition.<sup>17</sup> The catalysts were prepared by a chemical reduction method under microwave irradiation by using poly (N-vinyl-2-pyrrolidone) as a protective agent. The catalyst particles with the size of 0.5-3 nm produced single-walled carbon nanotubes in 200% higher yield than the unpromoted catalyst due to the synergetic effects of noble metals with iron on the silica surface. Shah et al.<sup>18</sup> reported methane decomposition over Mo Ni and Pd-promoted Fe/Al<sub>2</sub>O<sub>3</sub> catalysts and reported that the bimetallic catalysts showed better activity for methane decomposition. A hydrogen yield of above 80% was achieved over the bimetallic catalysts. However, the Pd-promoted catalyst showed an improved activity for hydrogen production and for the selective growth of carbon. Odier et al.<sup>19</sup> studied a Pt/CeO<sub>2</sub> catalyst for methane decomposition. An improved hydrogen production rate was noticed over the platinum catalyst due to spillover effects. However, because of the redox nature of ceria, CO<sub>x</sub> was detected in the hydrogen stream, possibly formed by the interaction of the lattice oxygen of ceria with the deposited carbon.<sup>13</sup>

In another work, Prasad et al.<sup>20</sup> used 5% and 10% Pd-promoted activated carbon catalysts for methane decomposition. Among the catalysts, the 10% Pd-promoted catalyst exhibited high catalytic activity and stability at 850°C due to presence of more Pd crystals on the surface of activated carbon. A highest hydrogen production rate of ~0.3 and ~0.4–0.6 mmol/(min g) was observed for the 5 and 10% Pd-loaded AC catalysts, respectively. Moreover, carbon nanofibres with high crystallinity were deposited over the 10% Pd/AC catalyst after methane decomposition. Szymanska et al.<sup>21</sup> used Pt-, Pd- and Cr-supported activated carbon catalysts for methane decomposition. They reported that the Pd-based catalysts showed high catalytic efficiency with various loadings of 1, 5, 10 and 20%. When increasing the amount of Pd, the methane conversion increased, and no deactivation was observed. A maximum hydrogen production rate of 8 mmol/(min g) was observed over the 20% Pd catalyst. However, due to the presence of a very small amount of Pd on the activated carbon, the 1% Pd catalyst provided low activity for methane decomposition.

Takenaka et al.<sup>22</sup> studied methane decomposition over Ni/SiO<sub>2</sub>, Pd/SiO<sub>2</sub> and Ni-Pd/SiO<sub>2</sub> catalysts. They reported that the addition of Pd to the Ni/SiO<sub>2</sub> catalyst improved the activity and stability of the catalyst for methane decomposition. This could be due to the presence of highly dispersed Ni-Pd bimetallic alloys over the silica. However, the high catalytic stability of the catalysts could be attributed to the increased number of facets on the Pd-Ni alloys after the precipitation of supersaturated carbon. Nuernberg et al.<sup>23</sup> used Pt-promoted 15% Ni/MgAl<sub>2</sub>O<sub>4</sub> catalysts for methane decomposition and

reported that the catalytic activity of Ni/MgAl<sub>2</sub>O<sub>4</sub> was improved by the addition of a small amount of Pt as a promoter. As per their report, over a 0.1% Pt-promoted catalyst, a maximum methane conversion of 14% was observed in the initial stage of the reaction with a feed of 7:1 molar ratio of N<sub>2</sub>:CH<sub>4</sub> at 700°C. Punnoose et al.<sup>24</sup> investigated methane decomposition over bimetallic Fe-Pd and Fe-Mo catalysts supported over alumina. They reported that high catalytic activity was observed for the Pd-promoted bimetallic catalyst compared to their monometallic analogues at 700-800°C. The palladium-based bimetallic catalyst provided a maximum hydrogen yield of 80% compared to the other catalysts. Approximately 75% and 65% of hydrogen yield was obtained for the Fe-Mo and Fe-Ni bimetallic catalysts, respectively, at 700°C. In another work, Takenaka et al.<sup>14, 25</sup> used Pd-promoted Ni-, Fe-, and Cu-loaded alumina-supported bimetallic catalysts for methane decomposition. As per their results, the Pd-M/Al<sub>2</sub>O<sub>3</sub> (M = Fe, Co, Ni, Cu, Ag, and Rh) catalysts provided high methane conversions of 35-50% in the temperature range of 700-900°C with a gas space velocity of 160 l/h g. Moreover, the methane conversion decreased to 5-10% during the course of the reaction with a streaming time of 3-10 h.

Thus, it is clear that the metal promoters play a significant role in the catalytic performance of the catalysts. Also, it was found that Pd is widely studied in this process compared to other noble metals, especially platinum. Previously, our group had reported Pd-promoted nickel catalysts supported over MgAl<sub>2</sub>O<sub>4</sub> and SBA-15 for methane decomposition.<sup>15, 26</sup> Therefore, in the present study, we focused on the development of a set of Pt-promoted nickel catalysts with various loadings of Pt and their catalytic performance for methane decomposition. Herein, highly porous ceria were prepared by a urea-assisted solid state combustion method and used as a support for the Pt-promoted nickel catalysts with various amounts of Pt promoter. The as-prepared Pt-promoted ceria supported nickel catalysts were tested for the catalytic decomposition of methane. To the best of our knowledge, this type of catalyst composition is not yet reported in methane decomposition literature. Moreover, the prepared catalysts were completely characterized using several analytical methods, and their properties were correlated to their performance for methane decomposition. The catalysts provided high catalytic activity and stability for a period of 360 minutes of reaction without any deactivation. Moreover, the effect of Pt, its amount, reaction temperature and the structural and crystalline properties of the deposited carbon were investigated in detail.

## Experimental

### Synthesis of Pt promoted Ni/CeO<sub>2</sub> catalysts

All of the chemicals used in the experiments were of analytical grade and were purchased from R&M chemicals. A two-step synthesis was used to prepare the Pt-promoted Ni/CeO<sub>2</sub> catalysts. In the first step, the highly porous CeO<sub>2</sub> support was prepared via a solid state combustion method

using urea as a fuel, and, secondly, the active metal Ni and promoter Pt was incorporated into CeO<sub>2</sub> by a wet impregnation method. For the synthesis of the CeO<sub>2</sub> support, 0.1 mol of cerium nitrate hexahydrate and 0.5 mol of urea were mixed and grinded in a mortar using a pestle until it becomes a sticky paste. The material was then transferred to a quartz crucible and calcined at 700°C for 5 hours in a muffle furnace to obtain the CeO<sub>2</sub> support. For the preparation of nickel-loaded and Pt-promoted catalysts, the weighed amounts of the nickel nitrate hexahydrate and platinum tetrachloride (PtCl<sub>4</sub>, Aladdin, China) were dissolved in 500 mL of distilled water taken in a 1 L beaker and heated to 80-85°C with magnetic stirring. Next, the weighed amount of synthesized ceria was slowly added. After the complete addition of ceria, the solution was subjected to gentle evaporation at 85°C with magnetic stirring until it becomes a homogeneous paste. The paste was then carefully transferred into a quartz crucible and dried in an air driven oven at 100°C overnight. The dried sample was then crushed, powdered and calcined at 700°C for 5 hours to obtain the Pt-promoted Ni/CeO<sub>2</sub> catalysts. In the present synthesis, the amount of Ni was kept constant (20 wt %) in all of the catalysts, whereas the amount of Pt was varied as 0.05 wt%, 0.1wt% and 0.2 wt% by changing the amount of Pt precursor during the synthesis. The prepared support and catalysts were denoted as CeO<sub>2</sub>, Ni/CeO<sub>2</sub> and x%Pt@Ni/CeO<sub>2</sub>, where the x stands for the nominated amount of platinum in the catalyst.

### Materials characterization

The freshly prepared support, unpromoted and Pt-promoted Ni/CeO<sub>2</sub> catalysts were characterized for their crystalline, structural, morphological, textural and redox properties using different analytical methods, as reported in our previous works.<sup>27, 28</sup> The actual amount of metals in the fresh catalysts were studied using inductively coupling plasma - optical emission spectroscopy (ICP-OES). For ICP analysis, the metallic species were extracted in a hot acid mixture of HF, HCl and HNO<sub>3</sub> (1:1:3 volume ratio) at 50°C for 60 minutes, then diluted to pH 2 and analyzed. The crystallographic properties of the catalysts were studied using X-ray diffraction analysis, and the diffraction patterns were obtained with a Bruker D8 Focus X-Ray Diffractometer and were processed/analysed using EVA software. The samples were scanned in the range of 3-80° with a scan rate of 0.025°. Scherrer's equation was used to calculate the crystallite size of the metal oxides present in the fresh catalysts. The surface composition of the catalysts and its surface adsorbed species were studied using Fourier transform infrared (FTIR) spectroscopy, and the FTIR spectra were taken in transmission mode in the region of 400-4000 cm<sup>-1</sup> in a Thermoscientific NICOLET 6700 system. The morphology of the fresh catalysts was viewed using a ZEISS MERLIN COMPACT field emission scanning electron microscope (FESEM). The SEM micrographs of the catalysts were taken at an accelerating voltage of 3 kV. An Energy dispersive X-ray (EDX) analyser coupled with the SEM instrument was used to study the qualitative and quantitative composition of the catalysts. The transmission electron

## ARTICLE

Journal Name

microscopic (TEM) images of the catalysts were taken in a Philips CM-12 instrument, operated at a voltage of 100 keV for the determination of the internal morphology. The chemical structure and surface states of the elements in the fresh catalysts were determined using X-ray photoelectron spectroscopy (XPS) in a Kratos XSAM X-ray photoelectron spectrometer having a base pressure of  $10^{-9}$  Torr. The Mg K $\alpha$  X-radiation was used as the excitation source. The results were processed using vision processing software. The binding energy of C 1s (285 eV) was used as the reference to correct the charging shifts. A linear background subtraction was performed to present the results and the peaks in each spectrum were curve fitted using a Gaussian function. A Micromeritics ASAP 2020 surface area and porosity analyzer was used to study the textural properties of the catalysts. The Brunauer–Emmett–Teller (BET) method was used to calculate the specific surface area and, using the Barrett–Joyner–Halenda (BJH) method, the pore parameters such as pore size and pore volume were evaluated based on the desorption branch of the nitrogen isotherm. The samples were subjected to a degassing treatment at 300°C for 2 h. The hydrogen-temperature programmed reduction (H<sub>2</sub>-TPR) studies for the determination of the reduction behaviour of the catalysts were conducted in a Micromeritics Autochem 2920 chemisorption analyzer. The samples were reduced with 20 mL/min 10% H<sub>2</sub>/N<sub>2</sub> gas mixture from room temperature to 800°C with a heating rate of 10°C/min. Approximately 50 mg of each of the sample was used for the TPR experiments, and the consumption of hydrogen was monitored using a gas chromatograph equipped with a thermal conductivity detector. The carbon deposited catalysts after the methane decomposition reaction were further characterized using XRD, FESEM, TEM and TGA analyses. The thermogravimetric analysis was carried out in a Mettler Toledo thermogravimetric analyser (TGA/DSC1 model) under oxygen atmosphere.

### Methane decomposition experiments

Methane decomposition was studied as a test reaction to evaluate the catalytic performance of the Pt-promoted Ni/CeO<sub>2</sub> catalysts. The experiments were conducted in a vertical down flow stainless steel fixed bed reactor with a total length of 60 cm and internal and outer diameters of 2.5 and 3 cm, respectively. The reactor was heated by using an electric muffle furnace. The weighed amount of catalyst powder (2 g) was packed in the middle of the reactor using thermal resistant quartz wool and nitrogen was flushed to check the gas leakage (if any). After catalyst packing, the reactor temperature was increased from room temperature to reduction temperature (650°C) using a constant flow of nitrogen (150 mL/min). The nitrogen gas was replaced with hydrogen gas with a flow rate of 150 mL/min for 90 minutes for the catalyst reduction after attaining the reduction temperature. The hydrogen was discontinued after the catalyst reduction, and nitrogen was re-introduced to increase the reactor temperature to reaction temperature. Once attaining the reaction temperature, the nitrogen was shut off and methane was introduced into the reactor for the

decomposition reaction. The reaction was performed for 360 minutes on stream. During the reaction, the outlet gases were collected in gas sampling bags and were analysed by a Gas chromatograph (SRI GC 8610C) equipped with two packed columns (Molecular sieve 13X and Porapak Q) connected to a thermal conductivity detector using helium as the carrier gas. To report the catalytic performance of the catalysts for methane decomposition, hydrogen yield (%) was calculated. After 360 minutes of reaction, the reactor was cooled to room temperature with a constant flow of nitrogen (150 ml/min) to collect the carbon deposited catalysts for their characterization.<sup>29</sup>

## Results and Discussion

Table 1 shows the amount of metals in the fresh catalysts measured by ICP-OES analysis. A minimal variation was seen in the actual and nominated metal contents in the catalysts.

Catalysts	Nominated amount (Wt %)		Actual amount (ICP) (Wt %)	
	Ni	Pt	Ni	Pt
Ni/CeO <sub>2</sub>	20	0	17.3	0
0.05%Pt@Ni/CeO <sub>2</sub>	20	0.05	16.9	*ND
0.1%Pt@Ni/CeO <sub>2</sub>	20	0.10	19.2	0.088
0.2%Pt@Ni/CeO <sub>2</sub>	20	0.20	18.8	0.179

\*ND- Not detected

XRD analysis was used to study the crystallographic properties of the Pt-promoted Ni/CeO<sub>2</sub> catalysts, and the diffraction patterns are shown in Fig. 1.

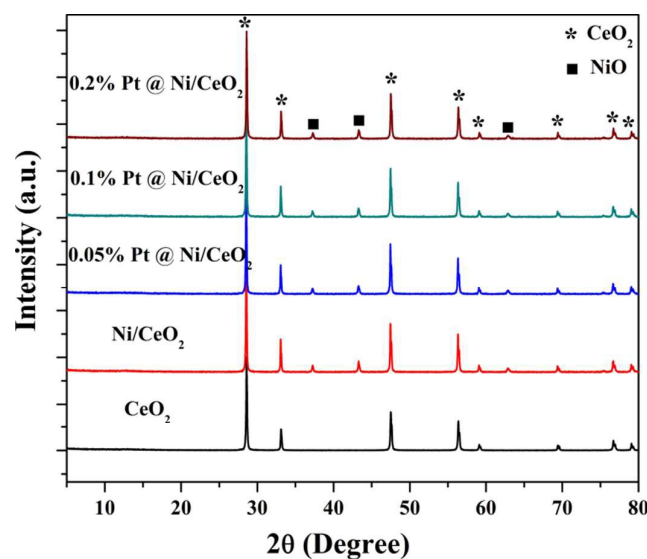


Fig. 1- X-ray diffraction patterns of the prepared catalysts

The diffraction peaks observed at the  $2\theta$  values of  $28.4^\circ$ ,  $33.1^\circ$ ,  $47.5^\circ$ ,  $56.4^\circ$ ,  $59.1^\circ$ ,  $69.4^\circ$ ,  $76.8^\circ$  and  $79.05^\circ$  were indexed to the presence of the face centred cubic phase crystalline structure of ceria. The other peaks observed at the  $2\theta$  values of  $37.3^\circ$ ,  $43.3^\circ$  and  $63^\circ$  were related to the presence of NiO in the catalysts. No peaks related to Pt were observed. The low intensity of the peaks of nickel oxide compared to the peaks of ceria and the absence of Pt peaks confirms the fine surface dispersion of NiO and Pt in the catalysts.<sup>30</sup> No formation of NiCeO solid solution was detected. The average crystallite size of ceria prepared by the urea-assisted solid state combustion method was calculated to be 24 nm, whereas the crystallite size of ceria after nickel loading was found to be slightly increased to 28 nm, as indicated by the intensity of the diffraction peaks. The presence of platinum and its amount did not contribute to the crystallite size of ceria in the Pt-promoted nickel catalysts, since the crystallite size of ceria was calculated to be same ( $28 \pm 1$  nm) in all of the nickel catalysts. The crystallite size of nickel oxide was not calculated because of the low intensity of the peaks, which is not altered by the addition of Pt or with its amount. The low crystallinity of NiO further ensures the good homogenous surface dispersion of the nickel species in the catalysts.<sup>31</sup> No impurities were detected, as indicated by the absence of other unwanted peaks.

FTIR spectra of the support and Pt-promoted nickel catalysts were studied for the determination of their surface composition and functional groups present in the catalysts. As shown in Fig. 2, only one well resolved transmission band was observed in all of the samples. The transmission band observed at  $505\text{ cm}^{-1}$  could be attributed to the stretching vibration of the Ce-O bond, confirming the presence of  $\text{CeO}_2$ .<sup>32</sup> This band was retained in the catalysts, irrespective of the addition of nickel and platinum. The transmission band for NiO was not seen clearly and which is expected to merge with the Ce-O band. It further confirms the surface dispersion of NiO in the  $\text{CeO}_2$  support.<sup>33</sup>

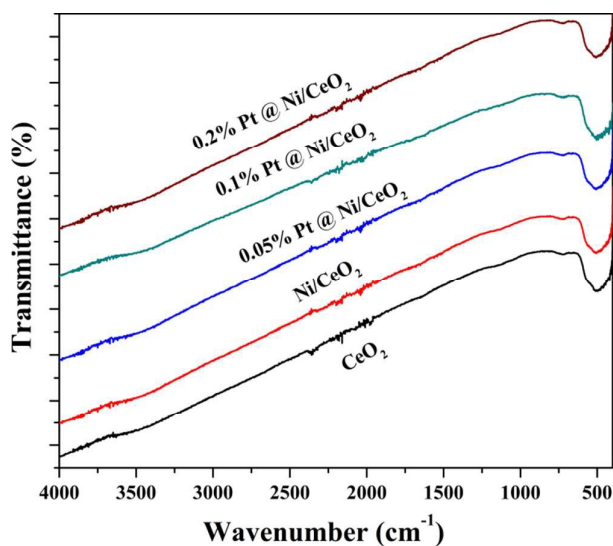


Fig. 2- FTIR spectra of the prepared catalysts

No other transmission band was detected in the catalysts, indicating the absence of surface-adsorbed impurities in the catalysts.

The surface morphology of the prepared support, unpromoted and Pt-promoted nickel catalysts were investigated using FESEM analysis, and the images are shown in Fig. 3.

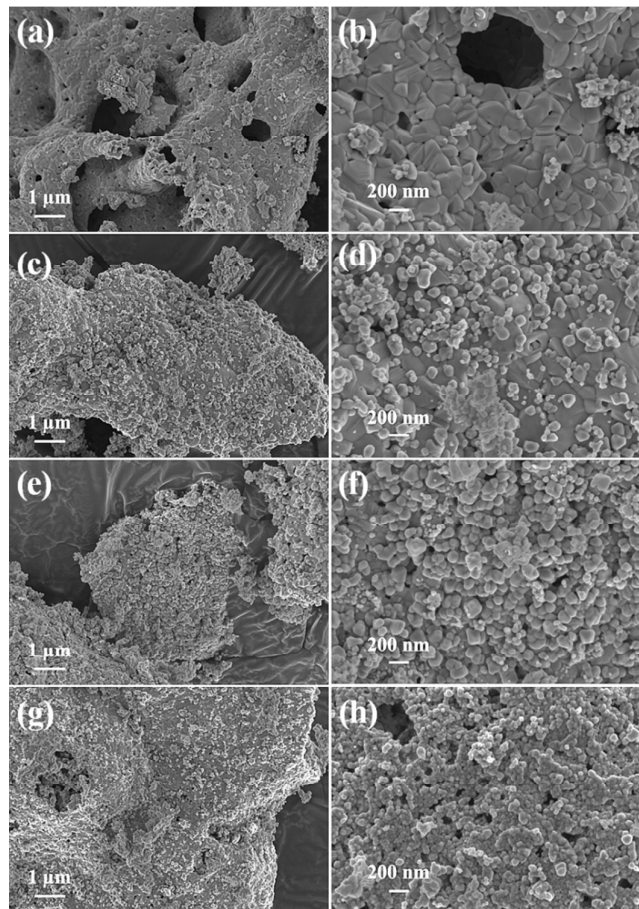


Fig. 3- SEM micrographs of the samples (a, b)  $\text{CeO}_2$ , (c, d) Ni/ $\text{CeO}_2$ , (e, f) 0.1 %Pt@Ni/ $\text{CeO}_2$  and (g, h) 0.2%Pt@Ni/ $\text{CeO}_2$  catalysts

The urea-assisted solid state combustion derived  $\text{CeO}_2$  support exhibited a homogeneous porous structure. The  $\text{CeO}_2$  support seems like a porous sponge where a number of pores with different sizes were observed. These cave like- pores could be developed due the release of gases from the bulk of the mixed sample during combustion process. The high magnification image in Fig. 3(b) shows the presence of homogeneously aggregated polygonal shaped  $\text{CeO}_2$  nanoparticles. The sizes of the  $\text{CeO}_2$  particles were found to be varied on the nanoscale, and they were tightly aggregated. In addition to the existence big pores in the catalysts, the inter-aggregation of the polygonal shaped particles resulted in the development of some tiny voids in the sample. However, these

## ARTICLE

Journal Name

kinds of pores were not seen consistently in the sample due to the high degree of tight aggregation of ceria particles.

The surface of the ceria support was found to be covered with metal species after nickel and Pt-loading in the catalysts, which further confirms the homogenous dispersion of metal species over the ceria.<sup>34</sup> In the Ni/CeO<sub>2</sub> catalyst, the nickel oxide particles were observed to exist in the form of quasi-spheres and are not significantly aggregated as in the Pt-promoted catalysts (Fig. 3(c,d)). The surface of ceria is still visible together with the metal oxide particles. Pseudo-spherical particles of NiO were seen in the 0.1% Pt-promoted nickel catalysts. However, the surface of ceria was not seen in the Pt-promoted catalysts, which is completely covered with the metal species. The amount of Pt has a marked influence in the surface morphology of the Ni/CeO<sub>2</sub> catalyst. As shown, an aggregation of nanoparticles without any particle coagulation was seen over the 0.1% Pt-promoted catalyst (Fig. 3(e,f)). In contrast, in the 0.2% Pt-promoted catalyst, the particles were agglomerated considerably, which further provided a porous texture to the catalyst (Fig. 3(g, h)). Even though the size of the particles decreased after Pt addition, no change in the NiO crystallinity was detected because of their agglomeration, as observed in XRD analysis.

The quantitative and qualitative compositions of some of the representative samples were studied using EDX analysis, and the spectra are shown in Fig. SD1. As shown, only Ce and O, Ce, Ni and O and Ce, Ni, Pt and O were seen in the CeO<sub>2</sub>, Ni/CeO<sub>2</sub> and 0.2%Pt@Ni/CeO<sub>2</sub> catalysts, respectively. No other elements were detected in the samples, demonstrating the purity of the prepared catalysts.

The amount of Ni and Pt in the catalysts was determined from 5 different spots of the sample while performing the SEM-EDX analysis of the representative samples. The mean value of the amount of Ni and Pt was found to be 18.6 wt% and 20.7 wt% for Ni and O and 0.23% for the Pt in the Ni/CeO<sub>2</sub> and 0.2%Pt@Ni/CeO<sub>2</sub> catalysts, respectively. These values are in good agreement with the values of the metals in the catalysts. However, a minimal variation was observed in the values, which is in an acceptable range. The elemental mapping analysis of the 0.2% Pt-promoted nickel catalyst is shown in Fig. SD2. As shown, the metal species such as Ni and Pt were found to be highly dispersed on the catalyst.

The internal morphology of the representative catalysts was captured using TEM, and the micrographs are shown in Fig. 4. As shown, the catalysts showed aggregated particles in both of the samples. The sizes of particles were found to be quite large in the unpromoted catalyst, whereas, after Pt addition, the size of catalyst particles decreased, as shown in the images. The average sizes of the particles were measured to vary from 50-100 nm and 30-70 nm for the Ni/CeO<sub>2</sub> and 0.2%Pt@Ni/CeO<sub>2</sub> catalysts, respectively. Moreover, the Pt promotion increased the rate of homogenous aggregation of particles, as is consistent with the SEM results. The inter-aggregation of these catalyst particles could be responsible for the porous texture in the catalysts.

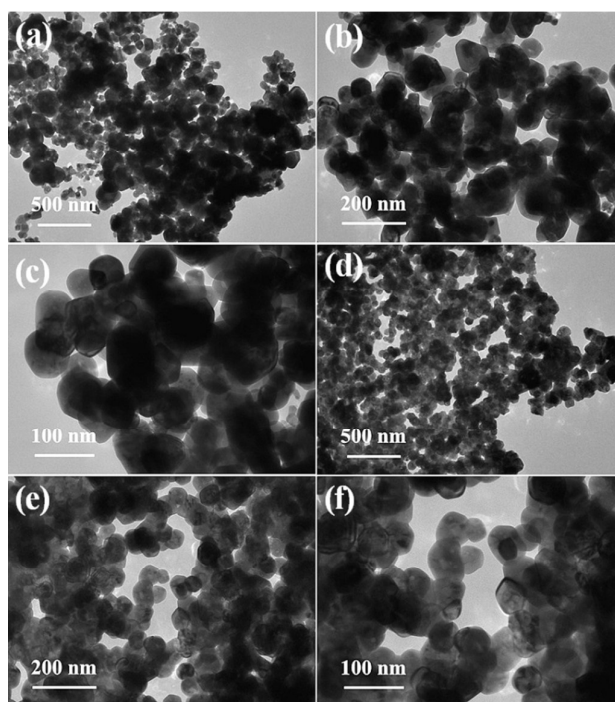


Fig. 4- TEM micrographs of the fresh catalysts: (a-c) Ni/CeO<sub>2</sub> and (d-f) 0.2 %Pt@ Ni/CeO<sub>2</sub> catalyst

The surface states and chemical bonding of the catalysts, was studied using XPS analysis, and the results are shown in Fig. 5. The wide scan XPS spectra indicated the presence of Pt, Ni, Ce, O and C as the main elements in the catalysts (Fig. 5(a)). The peak for C originated from the XPS measurement, which cannot be avoided in XPS analysis. The binding energy of C 1s, 285 eV, was used as the reference to correct the charging shifts. No other elements were detected, indicating the purity of the prepared catalyst.

High resolution elemental spectrum and the deconvoluted peaks of the 0.2%Pt@Ni/CeO<sub>2</sub> catalyst were studied in detail. Fig. 5(b) shows the high resolution spectrum of Pt 4f. Two peaks were detected with binding energies of 71.05 eV and 74.17 eV. These peaks correspond to Pt 4f7/2 and Pt 4f5/2, respectively, confirming the presence of platinum in its 0 oxidation state.<sup>35</sup> The deconvoluted Ni 2p spectrum is shown in Fig. 5(c). The peaks were fitted by considering two spin orbit doublets and two shake up satellites. The peaks fitted at the binding energies of 851.2 - 867.5 eV with a main peak at 854.4 eV and a satellite peak at 860.9 eV and the peaks fitted located at 868.5 - 884.1 eV with a main peak at 873.3 eV and a satellite peak at 879.4 eV were assigned to the Ni 2p3/2 and Ni 2p1/2 spin-orbit levels of NiO, respectively.<sup>36, 37</sup> The main peaks of Ni 2p located at the binding energies of 854.4 and 873.3 eV were in good agreement with the reported values of the +2 oxidation state of nickel.<sup>38</sup> In addition to these peaks, an additional shoulder peak appeared at 855.9 eV, which is probably due to the presence of a small amount of Ni in the +3 oxidation state on the surface the catalyst.<sup>37</sup>

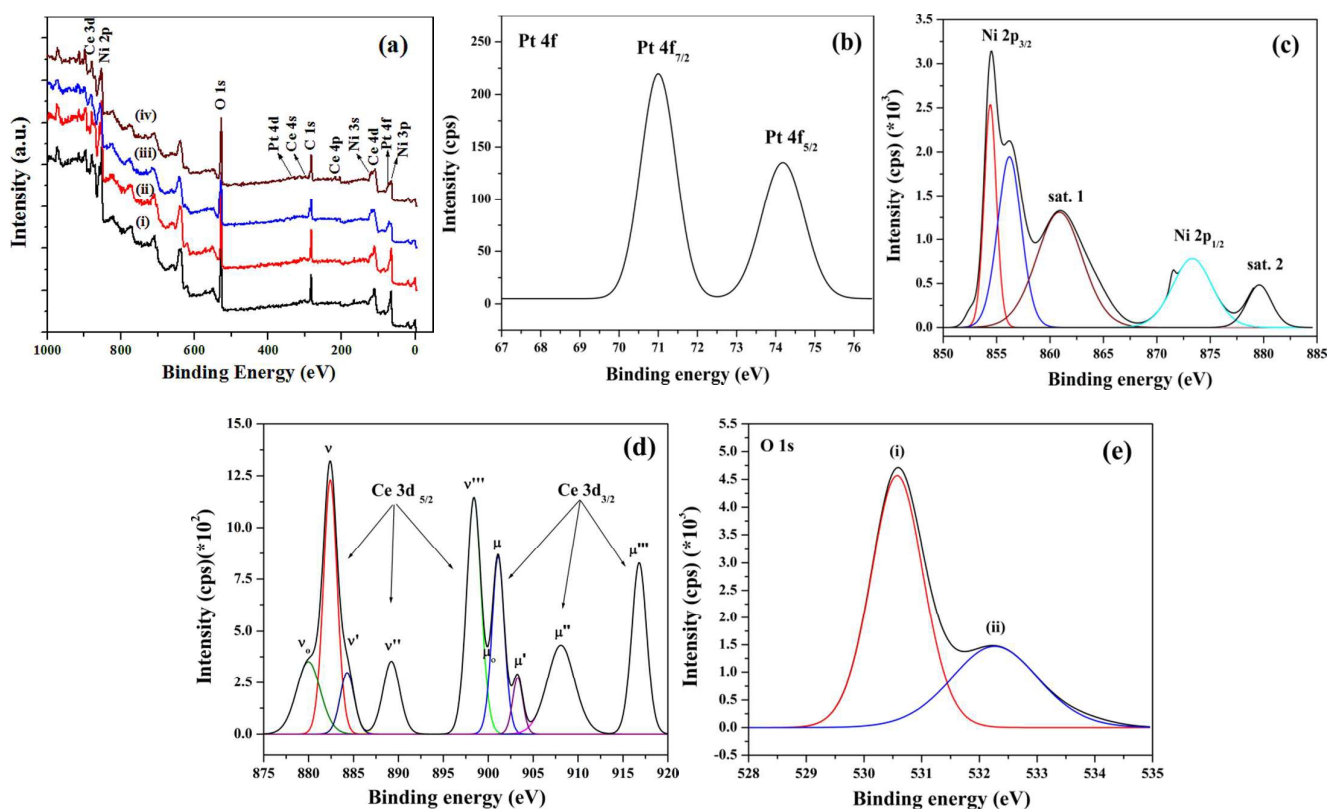


Fig. 5- XPS analysis of the catalysts: (a) Survey spectra of the prepared catalysts and the high-resolution XPS spectra and corresponding deconvoluted spectra of (b) Pt 4f, (c) Ni 2p, (d) Ce 3d and (e) O 1s in the 0.2% Pt@Ni/CeO<sub>2</sub> catalyst

The deconvoluted XPS spectra of the Ce 3d are shown in Fig. 5(d). Ceria is reported to be showing a core level spectrum with three resolved lobed envelopes because of its different final states of mixed valence.<sup>39, 40</sup> The lobed envelopes were observed at the binding energies 875.1-892.5 eV, 895-912.5 eV and 916.8 eV. The marked labels were identified as the Ce 3d peaks, where the “u” and “μ” represent the spin-orbit coupling of the Ce 3d<sub>5/2</sub> and Ce 3d<sub>3/2</sub> levels, respectively.<sup>41, 42</sup> The peaks observed at the binding energies of 882.4 eV (v), 889.24 eV (v’), 898.34 eV (v’'), 901.05 eV (u), 908.08 eV (u’), 916.73 eV (u’’) were ascribed to the +4 oxidation state of cerium (Ce<sup>4+</sup>), whereas the peaks at the binding energies of 879.89 eV (v<sub>0</sub>), 884.47 eV (v’<sub>0</sub>), 899.97 eV (u<sub>0</sub>) and 903.6 eV (u’<sub>0</sub>) were related to the +3 oxidation state of cerium (Ce<sup>3+</sup>).<sup>43,44</sup> The deconvoluted high-resolution XPS spectrum of O 1s is shown in Fig. 5(e). Two oxygen contributions were seen in the spectrum, as indicated by the two deconvoluted peaks. The fitting peak observed at the binding energy of 530.5 eV could be attributed to the oxygen bonded with the metal.<sup>38</sup> The second fitting peak of O1 at the binding energy of 532.26 eV could be due to the presence of a high number of defect sites with low oxygen coordination in the material.<sup>45</sup>

The textural properties of the support and Pt-promoted nickel catalysts were studied using BET/BJH analysis, and the adsorption-desorption isotherms are shown in Fig. 6.

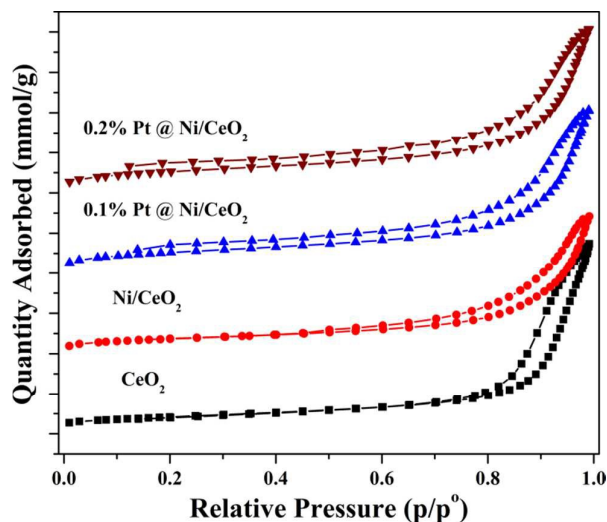


Fig. 6- BET-nitrogen adsorption-desorption isotherms of the prepared samples

The isotherms were classified as type IV according to the IUPAC classification. A H3 hysteresis loop can be observed in all of the catalysts, indicating the existence of mesopores in the prepared samples.<sup>46</sup> In ceria, the hysteresis loops were observed at the relative pressure range of 0.8 to 1. After nickel loading and Pt addition, the hysteresis loop was found to start quite early, as shown in the isotherms. The specific surface area, average pore size and average pore volume of the samples are tabulated in Table. 1. The specific surface area of the ceria prepared by the urea-assisted combustion method was measured to be 94.6 m<sup>2</sup>/g. After nickel loading, the surface area of the ceria catalyst was decreased to 58.29 m<sup>2</sup>/g. This could be due to the blocking of mesopores of ceria by the nickel oxide particles.<sup>47</sup> However, the addition of platinum significantly increased the surface area of the catalysts. By increasing the amount of Pt from 0.1% to 0.2%, the surface area of the catalyst was found to increase from 69.4 m<sup>2</sup>/g to 73.81 m<sup>2</sup>/g. Similar results were previously reported in the case of noble metal-promoted metal catalysts.<sup>48</sup> The synergistic effects of Pt and Ni could be the reason for this behaviour. Moreover, the average pore size of ceria (15.2 nm) was found to be not altered greatly even after nickel loading and Pt addition. However, the mean pore volume of ceria decreased from 0.3125 cm<sup>3</sup>/g to 0.2384 cm<sup>3</sup>/g after nickel loading, whereas, after Pt addition, it increased significantly according to the amount of Pt. By increasing the amount of Pt, the pore volume of the catalysts increased, as shown in Table. 1. The increased pore volume could be responsible for the high surface area of the catalysts.

the reduction temperatures. This is attributed to the hydrogen spillover effect of Pt with nickel species.<sup>48, 52</sup> The low temperature reduction peak of ceria due to surface oxygens is expecting to merge with NiO peaks. No high temperature reduction peaks were observed, indicating the absence of a strong metal support interaction.<sup>53</sup> This is highly consistent with the XRD observation of the absence of the NiCeO solid solution. The low temperature reduction peaks further confirm the homogenous dispersion of NiO on the surface of ceria.

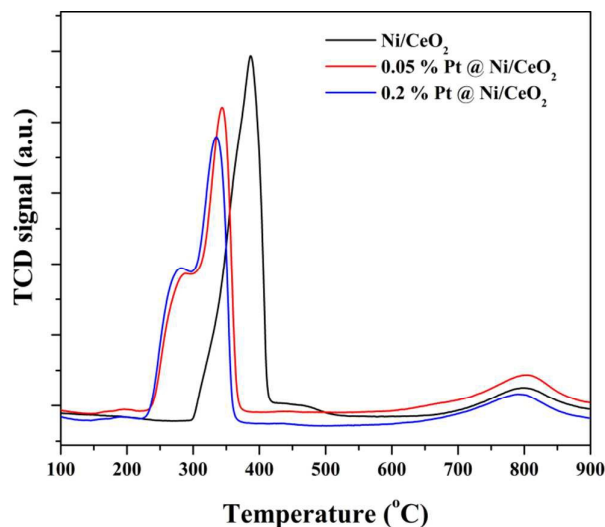


Fig. 7- TPR profiles of the fresh catalysts

Table 1- Textural properties of the ceria support, unpromoted and Pt promoted nickel catalysts

Catalysts	BET specific surface area (m <sup>2</sup> /g)	Pore size (nm)	Pore volume (cm <sup>3</sup> /g)
CeO <sub>2</sub>	94.61	15.2	0.3125
Ni/CeO <sub>2</sub>	58.29	14.4	0.2384
0.1%Pt@Ni/CeO <sub>2</sub>	69.40	13.9	0.2747
0.2%Pt@Ni/CeO <sub>2</sub>	73.81	14.7	0.2896

The reducibility of the unpromoted and Pt-promoted nickel catalysts were studied using TPR analysis, and the reduction profiles are shown in Fig. 7. Two resolved reduction peaks were observed in all of the catalysts. The first reduction peak centred at 386°C in the Ni/CeO<sub>2</sub> catalyst could be attributed to the reduction of isolated NiO, which is weakly interacted with the ceria support.<sup>49, 50</sup> The second broad reduction peak centred at nearly 800°C was ascribed to the reduction of the lattice oxygens of ceria.<sup>51</sup> After the addition of the Pt promoter, the reduction temperature of the samples was found to be shifted to low temperatures, as shown in the figures. A broad reduction peak starting from 225°C to 377°C with two maximas at 284°C and 343°C and 279°C and 335°C was observed for the 0.05% and 0.2% Pt promoted catalysts respectively. The increasing amount of Pt slightly decreased

The catalytic activity of the unpromoted and Pt-promoted nickel catalysts were tested for methane decomposition. The yield of hydrogen as a function of time on the stream over the prepared catalysts is plotted in Fig. 8. The catalysts showed high activity and stability for the decomposition reaction for a period of 360 minutes on the stream. The difference between the highest initial and final hydrogen yield was found to be very small, indicating the high stability of the catalysts. Only hydrogen and unreacted methane were detected in the reaction product, except for the unpromoted Ni/CeO<sub>2</sub> catalyst. Trace amounts of CO was observed in the outlet gas at the first 5 and 10 minutes of reaction over Ni/CeO<sub>2</sub> catalyst. However, no formation of CO or CO<sub>2</sub> was observed in the products in the Pt promoted catalysts, indicating the complete reduction of catalyst in the reduction process, which is promoted the

presence of Pt in the catalyst with its hydrogen spillover effects. Previously, Tang et al.<sup>13</sup> reported the formation of CO in methane decomposition due to the presence of the lattice oxygen of ceria, which could react with the deposited carbon.

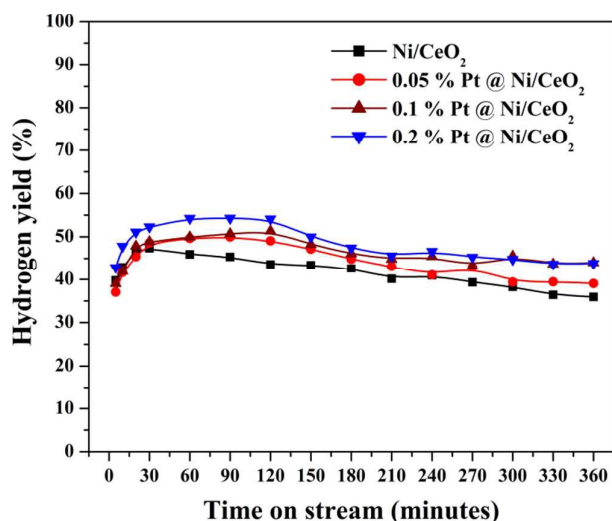


Fig. 8- Catalytic performance of the catalysts for methane decomposition: Effect of Pt and its amount (Reduction temperature-650°C, Reaction temperature-700°C, Catalyst weight- 2 g, Methane flow rate- 150 ml/min and Reaction time- 360 min)

The unpromoted nickel catalyst showed a maximum hydrogen yield of 46% at the first 30 minutes on the stream and, during the course of the reaction, it slightly decreased; at the end of 360 minutes, 36% hydrogen yield was observed. The addition of Pt as a promoter to the catalyst increased the hydrogen yield. Approximately 51% hydrogen yield was observed for the 0.05% Pt-promoted catalyst in the initial stage of the decomposition reaction, whereas, at the end of 360 minutes, 39% hydrogen yield was observed. The activity of the 0.1% Pt-promoted catalyst was found to be close to that of the 0.05% Pt-promoted catalyst until 210 minutes on the stream. Nearly 45% hydrogen yield was measured at 180 minutes on the stream and, after that, it remained more or less the same (45±1%) over the whole period of reaction. A maximum hydrogen yield of 54±1% was observed for the 0.2% Pt-promoted catalyst at 60 minutes on the stream. The activity remained the same until 120 minutes on the stream. After a gradual decrease of the hydrogen yield to 47%, it remained very close to the hydrogen yield obtained for the 0.1% Pt-promoted catalyst. At the end of 360 minutes, 45% hydrogen yield was measured. Thus, it can be said that the Pt-promoted catalysts provided more activity for methane decomposition compared to the unpromoted catalyst. This could be due to the synergistic effects of Pt and Ni over ceria. The addition platinum improved the surface area, pore parameters, and reduction behaviour of the Ni/CeO<sub>2</sub> catalyst. In addition, it promoted the surface dispersion of active metal particles on

the ceria. This could be responsible for the high performance of the Pt-promoted catalysts.

The effect of reaction temperature was also investigated using the 0.2% Pt-promoted catalyst. As shown in Fig. 9, by increasing the reaction temperature from 650°C to 750°C, the hydrogen yield also increased. This could be ascribed to the endothermic nature of the reaction. At 650°C, a maximum hydrogen yield of 47% was observed in the first 30 minutes on the stream, and, after a gradual decrease, nearly 39% hydrogen yield was measured at the end of 360 minutes of reaction. When the reaction temperature was increased by 50°C, the highest initial hydrogen yield of 55% and a final hydrogen yield of 45% were observed (700°C). At 750°C, a maximum hydrogen yield of 65% was observed at the first 30 minutes on the stream. The activity continued the same until 180 minutes on the stream. After that, a slow decrease in hydrogen yield was observed until 360 minutes on the stream, and nearly 55% hydrogen yield was observed at the end of 360 minutes. The high stability of the catalysts for methane decomposition at high temperatures could be due to the presence of highly dispersed nickel particles on ceria facilitated by the Pt promoter.

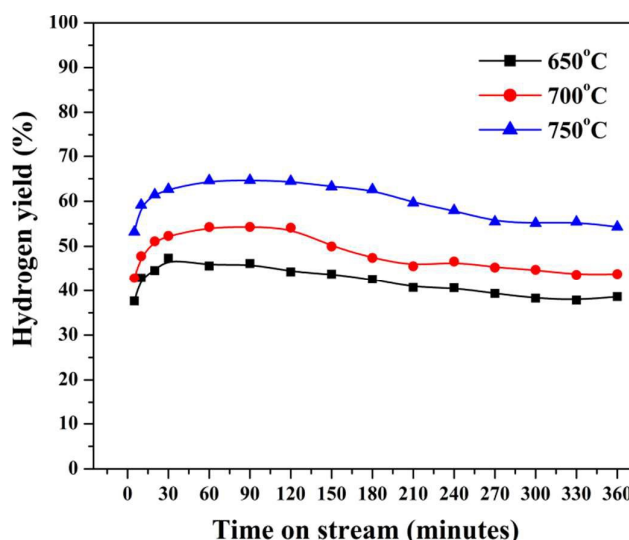


Fig. 9- Effect of reaction temperature on the hydrogen yield over 0.2% Pt @ Ni/CeO<sub>2</sub> catalyst (Reduction temperature 650°C, Catalyst weight- 2 g, Methane flow rate- 150 ml/min and Reaction time- 360 min)

For a comparative study, some of the recently reported metal catalysts for methane decomposition are discussed below. Al-Fatesh et al.<sup>54</sup> studied methane decomposition over alumina-supported Ni-, Co- and Fe-based mono, bi and trimetallic catalysts. They reported that the 15% Co-30% Fe/Al<sub>2</sub>O<sub>3</sub> catalyst showed a maximum hydrogen yield of 72% at 180 minutes on the stream. The hydrogen yield was found to be unaffected with the incremental addition of Co in the catalyst. Moreover, the addition of 10-20% Ni to the 30% Fe/Al<sub>2</sub>O<sub>3</sub> catalyst yielded a maximum hydrogen yield of 70%.

The trimetallic catalyst with a composition of 10% Ni-5% Co-30% Fe/Al<sub>2</sub>O<sub>3</sub> provided high catalytic efficiency for methane decomposition. Fakeeha et al.<sup>55</sup> studied methane decomposition over 12.5% Ni-12.5% Co loaded La<sub>2</sub>O<sub>3</sub> catalyst prepared by a co-precipitation method. At 700°C, nearly 80% hydrogen yield was achieved for the bimetallic catalyst, which was calcined at 500°C, and high catalytic stability was observed for a period of 300 minutes on the stream. In another work, Khan et al.<sup>56</sup> studied the catalytic decomposition of methane using lanthana-supported Ni- and Co-based bimetallic catalysts prepared by a co-precipitation method. A maximum hydrogen yield of 90% was observed over the 12.5Ni-12.5Co/La<sub>2</sub>O<sub>3</sub> catalyst at 300 minutes on the stream at a reaction temperature of 700°C. Moreover, the catalysts provided high catalytic stability for 24 h of reaction. In another work, Fakeeha et al.<sup>57</sup> reported methane decomposition over Ni- and Co-based bimetallic alumina catalysts prepared by a co-precipitation route and stated that a maximum methane conversion of 69% and 74% was observed in the initial and final periods of reaction, respectively, over the 25% Ni-25% Co/Al<sub>2</sub>O<sub>3</sub> catalyst. Zardin and Lopez<sup>58</sup> reported methane decomposition over a Co-Al mixed oxide catalyst synthesized by a co-precipitation method. According to their results, irrespective of the Co/Al ratio, the methane activated catalyst exhibited high catalytic activity and stability for the reaction. The highest methane conversion of 80% was achieved at 750°C.

Ahmed et al.<sup>59</sup> reported 50% Ni/CeO<sub>2</sub>-Al<sub>2</sub>O<sub>3</sub> catalysts with different loadings of ceria for methane decomposition. The amount of ceria in the catalyst played a significant role in the catalytic performance. The maximum hydrogen yield of ~53% was obtained over the Ni/Ce25-Al75 catalyst. Moreover, the highest catalytic stability was shown by the Ni/CeO<sub>2</sub> catalyst due to the presence of surface-dispersed nickel particles over ceria. In another work, Mahmoudi et al.<sup>60</sup> studied methane decomposition over activated carbon derived from olive stones by chemical and physical activation processes. The reaction was reported to occur in the micropores of the catalysts. At all reaction conditions, both of the catalysts were deactivated after 70 minutes on the stream at 800°C-850°C due to the decreased surface area of the catalysts. Carrillo et al.<sup>61</sup> studied methane decomposition over MnOx-loaded yttria-stabilized zirconia catalysts. The catalysts were found to be highly stable, and a maximum methane conversion of 30% was observed at 950°C. In another work, Awadallah et al.<sup>62</sup> studied methane decomposition over 40% Ni-loaded ZSM-5(25), ZSM-5(400) and amorphous silica (AS) catalysts. The catalysts prepared by the impregnation method shown a maximum hydrogen yield of 77%, irrespective of the support. However, during the course of the reaction, the hydrogen yield decreased with respect to the support material. Among the synthesized catalysts, the Ni/ZSM-400 catalyst showed high catalytic stability due to the presence of surface-dispersed metal particles on ZSM, where the hydrogen yield was measured to be 62% at 180 minutes on the stream. In contrast, nearly 13% and 42% hydrogen yields were observed for the Ni/AS and Ni/ZSM-25 catalysts, respectively, at 180

minutes on the stream. Ashik et al.<sup>63</sup> studied methane decomposition over a Ni/SiO<sub>2</sub> catalyst prepared by a co-precipitation modified Stober method and reported that 18.87 mmol/g min methane conversion was observed at 650°C.

Iron- and copper-promoted Ni/Al<sub>2</sub>O<sub>3</sub> catalysts were also successfully used for methane decomposition by Bayat et al.<sup>64</sup> As per their report, the 50% Ni-10% Fe-Cu/Al<sub>2</sub>O<sub>3</sub> catalyst showed high catalytic stability for the reaction at 675°C and 750°C for a period of 600 minutes of reaction due to the synergistic effects of the simultaneous additions of copper and iron as promoters. Li et al.<sup>65</sup> reported Ni/SiO<sub>2</sub> and NiCu/SiO<sub>2</sub> catalysts prepared by a hetero-phase sol gel method for methane decomposition. A maximum methane conversion of 23% was achieved over 10% Cu-promoted catalyst at 650°C. In other work, Bayat et al.<sup>66</sup> used Al<sub>2</sub>O<sub>3</sub>-supported NiCu catalysts for methane decomposition. Per their report, at 750°C, a maximum methane conversion of 84% was obtained in the first few minutes on the stream over the 50% Ni-10% Cu/Al<sub>2</sub>O<sub>3</sub> catalyst. However, with increasing time on the stream, a slight decline in the methane conversion was observed. In contrast, at 675°C, a steady state methane conversion of 70% was observed until the end of the 700 minutes of reaction. In another work, Bayat et al.<sup>67</sup> reported the high catalytic stability of the 50% Ni-15% Pd/Al<sub>2</sub>O<sub>3</sub> catalyst for methane decomposition for a period of 600 minutes, with a maximum hydrogen yield of 75% at 675°C. The methane conversion was found increase to 90% when the reaction temperature was increased to 750°C. However, a slight deactivation was observed during the course of the reaction due to the deposition of carbon.

Kang and Lee<sup>68</sup> used highly stable nickel-carbon-B<sub>2</sub>O<sub>3</sub> core-shell structured catalysts for methane decomposition and reported that the highest methane conversion of ~90% was achieved over 13%Ni@C-B<sub>2</sub>O<sub>3</sub> catalyst at a reaction temperature of 850°C. 15 cycles of reaction were performed using the same catalyst, indicative of the excellent stability of the catalyst due to its core-shell structure. In another work, Tang et al.<sup>13</sup> used Fe/CeO<sub>2</sub> catalysts for methane decomposition. Because of the presence of highly dispersed iron nanoparticles on ceria, the 60% Fe/CeO<sub>2</sub> catalyst showed high activity and stability for methane decomposition compared to the unsupported iron catalyst. A maximum methane conversion of 80% was observed during the initial period of reaction, whereas a steady state methane conversion of 23% was observed at 750°C for a period of 720 minutes of methane decomposition. Wang and Lua<sup>69</sup> reported methane decomposition over Ni-Cu alloy nanoparticles obtained through the thermal decomposition of NiCu oxalates. As per their report, a maximum methane conversion of ~82% was achieved at 750°C over the Ni-Cu alloy catalyst with a nickel composition of 62.5%. Zhou et al.<sup>70</sup> used Fe/Al<sub>2</sub>O<sub>3</sub> catalysts with various loadings of iron prepared by a fusion and an impregnation method for methane decomposition. All of the catalysts exhibited high catalytic efficiency for the reaction, irrespective of the amount of iron in the catalyst and the method of synthesis. At 750°C, a steady state methane conversion of 70% was obtained for the Fe/Al<sub>2</sub>O<sub>3</sub> catalyst with

65% iron prepared by the fusion method. Shen and Lua<sup>71</sup> studied methane decomposition over Ni/TiO<sub>2</sub> catalysts prepared by a sol gel method and reported that, at 500°C, a highest carbon yield of 321.1 gC/gNi was attained. In other work, Lua and Wang<sup>72</sup> used trimetallic Ni-Cu-Co alloy particles for methane decomposition. Up to 750°C, all of the alloys with different metal compositions provided high catalytic activity. In contrast, above 800°C, a rapid decrease in the catalytic activity was noticed. In another work, Ibrahim et al.<sup>73</sup> used Fe/Al<sub>2</sub>O<sub>3</sub> catalysts prepared by a coprecipitation method for methane decomposition. According to their results, the Fe/Al<sub>2</sub>O<sub>3</sub> catalysts provided a maximum hydrogen yield of ~77% at 700°C. Moreover, the hydrogen yield was found to increase with an increasing amount of iron in the catalyst. Thus, it could be said that the Pt-promoted Ni/CeO<sub>2</sub> catalysts have shown superior or comparable activity with these catalysts.

The 360 minutes of the methane decomposition reaction yielded nearly 6.6 g, 6.4 g, 6.7 g, and 7.1 g of carbon over the unpromoted and 0.05%, 0.1% and 0.2% Pt-promoted Ni/CeO<sub>2</sub> catalysts, respectively. The amount of deposited carbon was found to be somewhat the same in the unpromoted and 0.05% and 0.1% Pt promoted catalysts, whereas quite high amount of carbon was deposited over 0.2%Pt@Ni/CeO<sub>2</sub> catalyst. This could be attributed to the increased catalytic activity of the catalyst compared to other catalysts. Thus, it can be said that the Pt-promoted Ni/CeO<sub>2</sub> catalysts are highly efficient for the reaction to produce hydrogen and carbon simultaneously.

Moreover, it was found that with increasing the reaction temperature from 650°C to 750°C, the amount of deposited carbon also increased significantly. Approximately 6.5 g, 7.1 g, and 8.9 g of carbon were deposited over the 0.2% Pt-promoted Ni/CeO<sub>2</sub> catalyst at 650°C, 700°C and 750°C, respectively. In this case, the amount of deposited carbon is directly proportional to their catalytic performance. That is, the higher the reaction temperature, the higher the catalytic activity and hence, higher the carbon deposition.

The spent catalysts were further characterized using XRD to study their crystalline properties, and the diffraction patterns are shown in Fig. 10. The diffraction peak centred at the 2θ value of 26.5° could be assigned to the presence of graphitic carbon.<sup>74</sup> The d-spacing of the crystalline carbon was calculated to be 0.3442 nm, 0.3369 nm, 0.3410 nm and 0.3458 nm for the unpromoted and 0.05%, 0.1% and 0.2% Pt-promoted catalysts, respectively. The values were found to be very close to the ideal distance between graphitic layers, indicating the high crystallinity of the deposited carbon.<sup>29, 75</sup> Additionally, the peaks for ceria and nickel were detected. Among the peaks, highest intensity was shown by ceria. As shown, the intensity of the peaks of nickel was found to be very low, and the peak intensity decreased in the platinum-promoted catalysts. This further confirms the presence of highly dispersed nickel particles on ceria and the promoting role of platinum for the homogeneous surface dispersion of nickel crystallites. The crystallite size of nickel was calculated to be 8 nm for the Ni/CeO<sub>2</sub> catalyst, whereas it was calculated to be 5±1 nm for the Pt-promoted catalysts. This small nickel crystallites dispersed on the ceria matrix could be responsible

for the high activity and stability of the catalysts for methane decomposition.

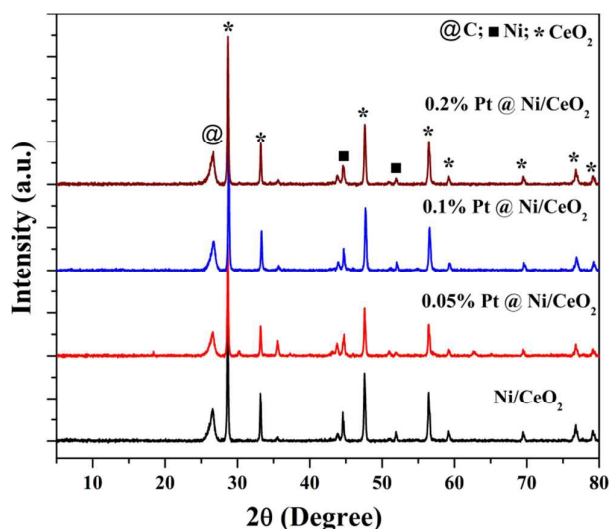


Fig. 10- XRD patterns of the spent catalysts

The spent catalysts were further characterized using thermogravimetric analysis and the TGA curves are shown in Fig. 11. As shown, single step weight loss was noticed for the spent catalysts. This could be due to the oxidative degradation of the deposited carbon. Since the oxidation started after 450°C, it is confirmed that there is no deposition of amorphous carbon. It is reported that the amorphous carbon oxidises before 400°C.<sup>76</sup> It further confirms the formation of crystalline carbon with high graphitization degree.

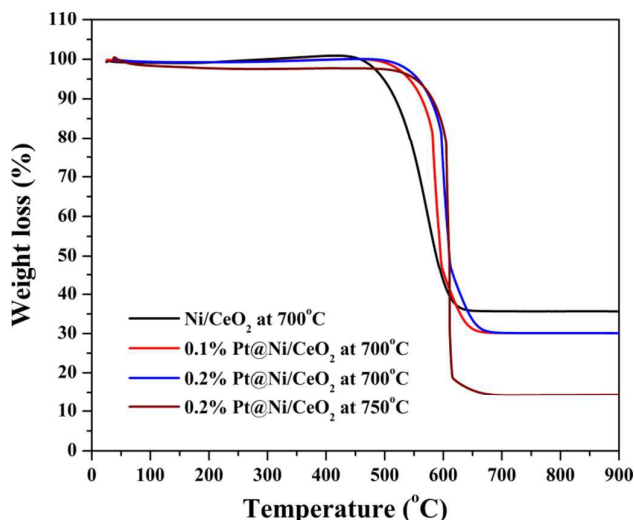


Fig. 11- TGA curves of the spent catalysts

The carbon yield was also calculated from TGA weight loss according to the equation: Carbon yield (%) = ((% of weight loss by carbon oxidation/% of residue after oxidation))\*

## ARTICLE

Journal Name

100.<sup>76,77</sup> The weight loss and carbon yield was measured to be 65%, 69.5% 70% and 84% and 186%, 228%, 233% and 525% for the Ni/CeO<sub>2</sub>, 0.1%Pt@Ni/CeO<sub>2</sub> and 0.2%Pt@Ni/CeO<sub>2</sub> catalysts at 700°C and 0.2%Pt@Ni/CeO<sub>2</sub> catalyst at 750°C respectively. Thus, it is clear that the addition of Pt as a promoter in the Ni/CeO<sub>2</sub> catalyst and with increasing the reaction temperature, a considerable increase in the carbon yield was noted. This is highly related to their catalytic activity. Moreover, it is found that the deposited carbon is highly crystalline because they were oxidized at high temperatures.<sup>27</sup>

The external morphology of the carbon-deposited catalysts was investigated using SEM analysis, and the micrographs are shown in Fig. 12. As shown, carbon was observed to be mainly deposited in the form of nanotubes. Bulk amounts of carbon nanotubes accumulated on the surface of the catalysts, as shown in the Fig. 12(a, d). The carbon nanotubes were found to be highly homogenous in diameter distribution and were interwoven. The diameters of the carbon nanotubes were measured a 20-30 nm in the unpromoted catalyst, while the diameters of the carbon nanotubes deposited over the Pt-promoted catalyst was varied greatly from 30-60 nm. However, the length of the carbon nanotubes was not possible to measure because of their intermixing in both of the catalysts. Compared to the carbon nanotubes deposited over the unpromoted catalyst, the carbon nanotubes deposited over the Pt-promoted catalyst seems to be denser and look like carbon nanowires.

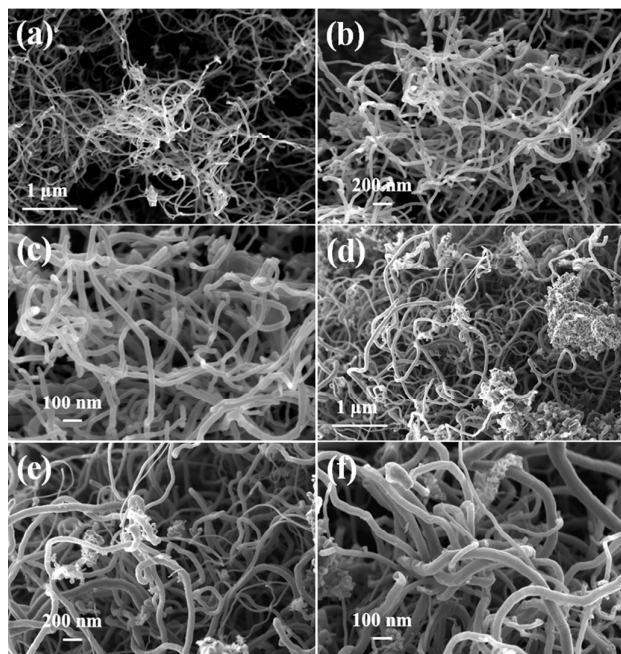


Fig. 12- SEM micrographs of the solid carbon deposited over (a-c) Ni/CeO<sub>2</sub> and (d-f) 0.2%Pt@Ni/CeO<sub>2</sub> catalysts

To evaluate the internal morphology in detail, TEM images were taken and are shown in Fig. 13. As shown, both carbon nanotube samples were multi-walled in nature. The outer wall thickness and internal channel space of the carbon nanotubes

shown in Fig. 13(b, d) were measured to be 5 nm and 10 nm and 6 nm and 14 nm for the unpromoted and Pt-promoted catalysts, respectively. Moreover, the Pt promoter increased the hollow structure of the carbon nanotubes by enhancing the width of the inner channel space of the carbon nanotubes.

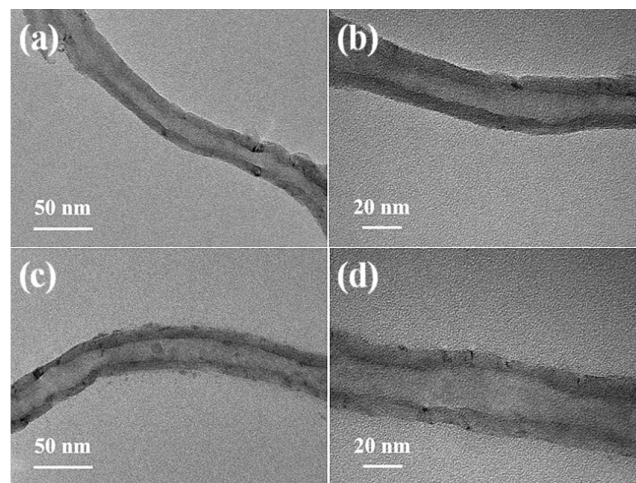


Fig. 13- TEM micrographs of the solid carbon deposited over (a-c) Ni/CeO<sub>2</sub> and (d-f) 0.2%Pt@Ni/CeO<sub>2</sub> catalysts

## Conclusions

In summary, a series of Pt-promoted nickel-ceria catalysts were successfully prepared by an impregnation method and used for methane decomposition. In the present study, rather than using commercial ceria, urea-assisted solid state combustion derived porous ceria was used as a catalyst support. Various characterization results indicated an enhanced role of the Pt and ceria support towards the catalytic activity of the catalysts. The active phase of nickel was found to be NiO, which was highly dispersed on the surface of the ceria. The addition of platinum as a promoter increased the metal oxide surface dispersion rate. The specific surface area of the Ni/CeO<sub>2</sub> catalyst increased with the addition of Pt, and with increasing amounts of Pt, the surface area of the Pt promoted catalyst was also increased considerably. This could be attributed to the synergistic effects of Pt and Ni over ceria. Moreover, the reduction temperatures were found to be lowered after Pt addition due to the hydrogen spillover effect. The scanning and transmission electron microscopic images indicated the presence of a porous network in the catalysts produced by the inter-aggregation of particles. The unpromoted and Pt-promoted catalysts provided high catalytic activity and stability for methane decomposition for a period of 360 minutes of reaction. The addition of platinum increased the hydrogen yield, and it increased with increasing amounts of Pt in the catalyst. Among the synthesized catalysts, the 0.2%Pt@Ni/CeO<sub>2</sub> catalyst showed the highest hydrogen yield. A maximum hydrogen yield of 65% was observed for the catalyst at 750°C. No catalyst deactivation or formation of CO<sub>x</sub> was detected, which might have been due to the enhanced

role of highly dispersed Pt and Ni nanoparticles over CeO<sub>2</sub> with the proper metal support interaction in the catalysts. Moreover, the effect of reaction temperatures studied in the range of 650°C to 750°C indicated that the hydrogen yield increased significantly with increasing reaction temperature. The carbon yield was also found to be increased with the incremental addition of Pt in the Ni/CeO<sub>2</sub> catalysts and also with increasing the reaction temperatures. A maximum carbon yield of 525% was achieved over 0.2%Pt@Ni/CeO<sub>2</sub> catalysts at 750°C. The characterization of spent catalysts indicated the deposition of highly crystalline multi-walled carbon nanotubes. The diameter distribution of the carbon nanotubes deposited over the platinum-promoted catalyst was found to vary considerably compared to the same deposit over the unpromoted catalyst. The addition of the Pt promoter increased the hollow structure of the carbon nanotubes since the measured internal channel space was quite high for the carbon nanotubes deposited over the Pt-promoted catalyst.

### Conflicts of interest

There are no conflicts to declare.

### Acknowledgements

This work was financially supported by Yayasan Sime Darby, Universiti Kebangsaan Malaysia and Sime Darby Research under grants PKT 6/2012 and KK-2014-014, respectively. The authors would like to thank the university administration for its support and FST and CRIM, UKM for performing the materials characterization. Manoj special thanks to Mr Mohamad Azri Tukimon, CRIM, UKM for providing the XPS analysis of the samples.

### References

- U.P.M. Ashik, W.M.A.W. Daud and H.F. Abbas, *Renewable Sustainable Energy Rev.* 2015, **44**, 221-256.
- T. Maneerung, K. Hidajat, S. Kawi, *Int. J. Hydrogen Energy* 2015, **40**, 13399-13411.
- J. Chi and H. Yu, *Chin. J. Catal.* 2018, **39**, 390-394.
- M. Pudukudy, Z. Yaakob, M. Mohammad, B. Narayanan, K. Sopian, *Renewable Sustainable Energy Rev* 2014, **30**, 743-757.
- A.M. Abdalla, S. Hossain, O.B. Nisfindy, A.T. Azad, M. Dawood, A.K. Azad, *Energy Convers. Manage.* 2018, **165**, 602-627.
- G. Guan, M. Kaewpanh, X. Hao, A. Abudul, *Renewable Sustainable Energy Rev.* 2016, **58**, 450-461.
- J.L. Pinilla, I. Suelves, M.J. Lázaro, R. Moliner, J.M. Palacios, *Appl. Catal., A* 2009, **363**, 199-207.
- D. Torres, J.L. Pinilla, M.J. Lázaro, R. Moliner, I. Suelves, *Int. J. Hydrogen Energy* 2014, **39**, 3698-3709.
- I. Suelves, J.L. Pinilla, M.J. Lázaro, R. Moliner, J.M. Palacios, *J. Power Sources* 2009, **192**, 35-42.
- H.F. Abbas, W.M.A.W. Daud, *Int. J. Hydrogen Energy* 2010, **35**, 1160-1190.
- Y. Li, D. Li, G. Wang, *Catal. Today* 2011, **162**, 1-48.
- U.P.M. Ashik, W.M.A.W. Daud, J. Hayashi, *Renewable Sustainable Energy Rev.* 2017, **76**, 743-767.
- L. Tang, D. Yamaguchi, N. Burke, D. Trimm, K. Chiang, *Catal. Commun.* 2010, **11**, 1215-19.
- S. Takenaka, Y. Shigeta, E. Tanabe, K. Otsuka, *J. Catal.* 2003, **220**, 468-477.
- M. Pudukudy, Yaakob Z, Akmal ZS. *Appl. Surf. Sci.* 2015, **353**, 127-136.
- H. Ogihara, S. Takenaka, I. Yamanaka, E. Tanabe, A. Genseki, K. Otsuka, *J. Catal.* 2006; **238**: 353-360.
- X. Wang, W.B. Yue, M.S. He, M.H. Liu, J. Zhang, Z.F. Liu. *Chem Mater* 2004, **16**, 799-805.
- N. Shah, D. Panjala, G.P. Huffman, *Energy Fuels* 2001, **15**, 1528-1534.
- E. Odier, Y. Schuurman, C. Mirodatos, *Catal. Today* 2007, **127**, 230-237.
- J.S. Prasad, V. Dhand, V. Himabindu, Y. Anjaneyulu, *Int. J. Hydrogen Energy* 2010, **35**, 10977-10983.
- M. Szymanska, A. Malaika, P. Rechnia, A. Miklaszewska, M. Kozłowski, *Catal. Today* 2015, **249**, 94-102.
- S. Takenaka, Y. Shigeta, E. Tanabe, K. Otsuka, *J. Phys. Chem. B.* 2004, **108**, 7656-7664.
- G.D.B. Nuernberg, H.V. Fajardo, E.L. Foletto, S.M.H. Probst, N.L.V. Carrenod, L.F.D. Probst, J. Barrault, *Catal Today* 2011, **176**, 465-469.
- A. Punnoose, N. Shah, G.P. Huffman, M.S. Seehra, *Fuel Process. Technol* 2003, **83**, 263-273.
- S. Takenaka, Y. Shigeta, K. Otsuka, *Chem. Lett.* 2003, **32**, 26-27.
- M. Pudukudy, Z. Yaakob, M.S. Takriff, *Appl. Surf. Sci.* 2015, **356**, 1320-1326.
- M. Pudukudy, Z. Yaakob, M.S. Takriff, *RSC Adv.* 2016, **6**, 68081-68091.
- M. Pudukudy, A. Kadier, Z. Yaakob, M.S. Takriff, *Int. J. Hydrogen Energy* 2016, **41**, 18509-18521.
- M. Pudukudy, Z. Yaakob, M.Z. Mazuki, M.S. Takriff, S.S. Jahaya, *Appl. Catal., B* 2017, **218**, 298-316.
- W. Liu, W. Wang, K. Tang, J. Guo, Y. Ren, S. Wang, L. Feng, Y. Yang, *Catal. Sci. Technol* 2016, **6**, 2427-2434.
- P. Zhao, F. Qin, Z. Huang, C. Sun, W. Shen, H. Xu. *Catal. Sci. Technol.*, 2018, **8**, 276-288.
- N. Maheswari, G. Muralidharan, *Dalton Trans.*, 2016, **45**, 14352-14362.
- S.B. Rathod, M.K. Lande, B.R. Arbad, A.B. Gambhire, *Arabian J. Chem.* 2014, **7**, 253-260.
- M. Pudukudy, Z. Yaakob, *Chem Eng. J* 2015, **262**, 1009-1021.
- C.R. Parkinson, M. Walker, C.F. McConville, *Surf. Sci.* 2003, **545**, 19-33.
- Z.A. Tan, W.Q. Zhang, D.P. Qian, C.H. Cui, Q. Xu, L.J. Li, S.S. Li, Y.F. Li, *Phys. Chem. Chem. Phys.* 2012, **14**, 14217-14223.
- Y.Q. Zhu, H.Z. Guo, Y. Wu, C.B. Cao, S. Tao, Z.Y. Wu, *J. Mater. Chem. A*, 2014, **2**, 7904-7911.
- C. Yuan, J. Li, L. Hou, Y. Long, L. Shen, X. Zhang, *J. Mater. Chem.*, 2012, **22**, 16084-16090.
- C.C. Hsieh, A. Roy, A. Rai, Y.F. Chang, S.K. Banerjee, *Appl. Phys. Lett.* 2015, **106**, 173108.
- H. Hasegawa, S.M.F. Shahed, Y. Sainoo, A. Beniya, N. Isomura, Y. Watanabe, T. Komeda, *J. Chem. Phys.* 2014, **140**, 044711.
- T. Alammar, H. Noei, Y. Wang, W. Grünert, A.V. Mudring, *ACS Sustainable Chem. Eng.* 2015, **3**, 42-54.
- Marrero-Jerez J, Larrondo S, Rodríguez-Castellón E, Núñez P. *Ceram Int* 2014, **40**, 6807-6814.
- B. Arndt, H. Noei, T.F. Keller, P. Müller, V. Vonk, A. Nanning, A.K. Opitz, J. Fleig, U. Rütt, A. Stierle. *Thin Solid Films* 2016, **603**, 56-61.
- X. Du, D. Zhang, L. Shi, R. Gao, J. Zhang, *J. Phys. Chem. C* 2012, **116**, 10009-10016.

## ARTICLE

Journal Name

- 45 V.M. Jimenez, A. Fernandez, J.P. Espinos, A.R.G. Elipe, *Journal of Electron Spectroscopy and Related Phenomena*, 1995, **71**, 61-71.
- 46 M. Möller, N. Tarabanko, C. Wessel, R. Ellinghaus, H. Over, B.M. Smarsly, *RSC Adv.* 2018, **8**, 132-144.
- 47 X. Zhang, L. Zhang, H. Peng, X. You, C. Peng, X. Xu, W. Liu, X. Fang, Z. Wang, N. Zhang, X. Wang, *Appl. Catal., B* 2018, **224**, 488-499.
- 48 L.P.R. Profeti, J.A.C. Dias, J.M. Assaf, E.M. Assaf, *J. Power Sources* 2009, **190**, 525-533.
- 49 X. Liao, Y. Zhang, M. Hill, X. Xia, Y. Zhao, Z. Jiang, *Appl. Catal. A: Gen.* 2014, **488**, 256-264.
- 50 V. Palma, C. Ruocco, A. Ricca, *Chem. Eng. Tran* 2015, **43**, 559-564.
- 51 L. Atzori, M.G. Cutrufello, D. Meloni, C. Cannas, D. Gazzoli, R. Monaci, M.F. Sini, E. Rombi, *Catal. Today* 2018, **299**, 183-192.
- 52 B.D. Adams, C.K. Ostrom, S. Chen, A. Chen, *J. Phys. Chem. C* 2010, **114**, 19875-19882.
- 53 S. Chettibi, Y. Benguedouar, N. Keghouche, *Physics Procedia*, 2009, **2**, 707-12.
- 54 A.S. Al-Fatesh, A.H. Fakeeha, W.U. Khan, A.A. Ibrahim, S. He, K. Seshan, *Int J Hydrogen Energy* 2016, **41**, 22932-22940.
- 55 A.H. Fakeeha, W.U. Khan, A.S. Al-Fatesh, A.A. Ibrahim, A.E. Abasaeed, *Int J Hydrogen Energy* 2016, **41**, 8193-8198.
- 56 W.U. Khan, A.H. Fakeeha, A.S. Al-Fatesh, A.A. Ibrahim, A.E. Abasaeed, *Int J Hydrogen Energy* 2016, **41**, 976-983.
- 57 A.H. Fakeeha, W.U. Khan, A.S. Al-Fatesh, A.E. Abasaeed, M.A. Naeem, *Int J Hydrogen Energy* 2015, **40**, 1774-1781.
- 58 L. Zardin, O.W.P. Lopez, *Int J Hydrogen Energy* 2017, **42**, 7895-7907.
- 59 W. Ahmed, A.E. Awadallah, A.A. Aboul-Enein, *Int J Hydrogen Energy* 2016, **41**, 18484-18493.
- 60 M. Mahmoudi, J. Dentzer, R. Gadiou, A. Ouederni, *Int J Hydrogen Energy* 2017, **42**, 8712-8720.
- 61 A.J. Carrillo, D. Sastre, L. Zazo, D.P. Serrano, J.M. Coronado, P. Pizarro, *Int J Hydrogen Energy* 2016, **41**, 19382-19389.
- 62 A.E. Awadallah, D.S. El Desouki, N.A.K.A. Gheit, A.H. Ibrahim, A.K.A. Gheit, *Int J Hydrogen Energy* 2016, **41**, 16890-16902.
- 63 U.P.M. Ashik, W.M.A.W. Daud, H.F. Abbas, *Int J Hydrogen Energy* 2017, **42**, 938-952.
- 64 N. Bayat, F. Meshkani, M. Rezaei, *Int J Hydrogen Energy* 2016, **41**, 13039-13049.
- 65 J. Li, L. Dong, L. Xiong, Y. Yang, Y. Du, L. Zhao, et al. *Int. J. Hydrogen Energy* 2016, **41**, 12038-12048.
- 66 N. Bayat, M. Rezaei, F. Meshkani, *Fuel* 2017, **195**, 88-96.
- 67 N. Bayat, M. Rezaei, F. Meshkani, *Int. J. Hydrogen Energy* 2016, **41**, 1574-1584.
- 68 D. Kang, J.W. Lee, *Appl. Catal. B* 2016, **186**, 41-55.
- 69 H.Y. Wang, A.C. Lua, *Chem. Eng. J* 2015, **262**, 1077-1089.
- 70 L. Zhou, L.R. Enakonda, M. Harb, A.A.T.Y. Saih, S. Ould-Chikh, et al. *Appl. Catal., B* 2017, **208**, 44-59.
- 71 Y. Shen, A.C. Lua, *J. Power Sources* 2015, **280**, 467-475.
- 72 A.C. Lua, H.Y. Wang, *Appl. Catal., B* 2014, **156-157**, 84-93.
- 73 A.A. Ibrahim, A.H. Fakeeha, A.S. Al-Fatesh, A.E. Abasaeed, W.U. Khan, *Int. J. Hydrogen Energy* 2015, **40**, 7593-7600.
- 74 M. Pudukudy, Z. Yaakob, Z.S. Akmal, *Appl. Surf. Sci.* 2015, **330**, 418-430.
- 75 M. Pudukudy, Z. Yaakob, A. Kadier, M.S. Takriff, N.S.M. Hassan, *Int. J. Hydrogen Energy* 2017, **42**, 16495-16513.
- 76 A.E. Awadallah, A.A. Aboul-Enein, A.K. Aboul-Gheit, *Energy Convers. Manage.* 2014, **77**, 143-151.
- 77 A.E. Awadallah, M.S. Mostafa, A.A. Aboul-Enein, S.A. Hanafi, *Fuel*, 2014, **129**, 68-77.

## Graphical abstract

A series of Pt promoted Ni/CeO<sub>2</sub> catalysts were prepared, characterized and their catalytic activity for methane decomposition is reported.

